

## SUPERCONDUCTIVITY

# Nearly ferromagnetic spin-triplet superconductivity

Sheng Ran<sup>1,2\*</sup>, Chris Eckberg<sup>2</sup>, Qing-Ping Ding<sup>3</sup>, Yuji Furukawa<sup>3</sup>, Tristin Metz<sup>2</sup>, Shanta R. Saha<sup>1,2</sup>, I-Lin Liu<sup>1,2,4</sup>, Mark Zic<sup>2</sup>, Hyunsoo Kim<sup>2</sup>, Johnpierre Paglione<sup>1,2</sup>, Nicholas P. Butch<sup>1,2,\*</sup>

Spin-triplet superconductors potentially host topological excitations that are of interest for quantum information processing. We report the discovery of spin-triplet superconductivity in  $\text{UTe}_2$ , featuring a transition temperature of 1.6 kelvin and a very large and anisotropic upper critical field exceeding 40 teslas. This superconducting phase stability suggests that  $\text{UTe}_2$  is related to ferromagnetic superconductors such as  $\text{UGe}_2$ ,  $\text{URhGe}$ , and  $\text{UCoGe}$ . However, the lack of magnetic order and the observation of quantum critical scaling place  $\text{UTe}_2$  at the paramagnetic end of this ferromagnetic superconductor series. A large intrinsic zero-temperature reservoir of ungapped fermions indicates a highly unconventional type of superconducting pairing.

Topological superconductivity has attracted great interest in condensed matter physics because of its potential application for topological quantum computing (1–4). A promising platform for topological superconductivity and Majorana fermions is the spin-triplet superconducting pairing state. For instance, the earliest theoretical model system of topological superconductivity was a one-dimensional (1D) spinless p-wave superconductor, which hosts Majorana zero modes at the ends of the chain (5). In 2D spinless chiral p-wave superconductors, Majorana zero modes bind to the superconducting vortices (6). However, triplet pairing rarely exists in nature—only a dozen from the few thousand superconducting compounds discovered so far have been identified as candidate materials. Therefore, in the past decade, the experimental realization of topological superconductors has been sought in engineered topological phases, such as heterostructures in which triplet pairing is induced by proximity effect with conventional s-wave superconductors (7). Intrinsic triplet superconductors, where the pairing state emerges by virtue of the materials' internal properties, have been underexplored owing to the limited number of candidate compounds, such as  $\text{Sr}_2\text{RuO}_4$  (8–10) and  $\text{UPt}_3$  (11, 12).

Here, we report the discovery of a flavor of superconductivity in  $\text{UTe}_2$  that exhibits the crucial ingredients of a spin-triplet pairing state—namely, an extremely large, anisotropic upper critical field  $H_{c2}$ ; temperature-independent nuclear magnetic resonance (NMR) Knight shift; and power law behavior of electronic specific heat and

nuclear spin-lattice relaxation rate in the superconducting state. In addition,  $\text{UTe}_2$  closely resembles ferromagnetic superconductors, but with a dramatically enhanced transition temperature and upper critical field relative to known compounds (13–16), and a paramagnetic normal state; this suggests that  $\text{UTe}_2$  is the paramagnetic end member of a ferromagnetic superconductor series.

$\text{UTe}_2$  crystallizes in the orthorhombic, centrosymmetric structure (space group  $71\text{Immm}$ ). U atoms compose parallel linear chains oriented along the  $[100] a$  axis (Fig. 1C), which coincides with the magnetic easy axis, as seen in the magnetic susceptibility  $M/H$ , where  $M$  is magnetization and  $H$  is magnetic field strength (Fig. 2A). The low symmetry of this structure is responsible for the large magnetic anisotropy (17), similar to the anisotropy in the orthorhombic, ferromagnetic superconductors  $\text{URhGe}$  and  $\text{UCoGe}$  (14, 15). Unlike these compounds, or the isoelectronic compound  $\text{USe}_2$  (18), the temperature dependence of the magnetization and electrical resistivity show no indications of a phase transition to a magnetically ordered state (Fig. 2). The high-temperature magnetization data show paramagnetic behavior along all three crystallographic axes. A Curie-Weiss fit yields an effective moment of 2.8 bohr magnetons per unit ( $\mu_B/U$ ), reduced from the value of a fully degenerate  $5f^2$  or  $5f^3$  configuration. At low temperatures, the magnetization decreases along the  $b$  axis and becomes temperature-independent, a signature of Kondo coherence (19), whereas along the  $a$  axis the magnetization increases sharply and then shows a slight slope change at  $\sim 10$  K, likely thanks to the Kondo coherence as well. No indication of phase transition at 10 K is observed from specific heat (see fig. S10) or resistivity measurements (Fig. 2C).

The high-temperature electrical resistivity  $\rho(T)$  is typical of uncorrelated, paramagnetic moments in the presence of single-ion Kondo hybridization with the conduction band, which is respon-

sible for the negative slope. At temperatures below a crossover marked by maximal resistivity, the Kondo hybridization yields coherent electronic bands, resulting in a metallic temperature-dependence (Fig. 2C). Although  $\text{UTe}_2$  does not magnetically order, the low-temperature magnetic behavior shows that  $\text{UTe}_2$  is on the verge of ferromagnetism. Below 10 K, the  $a$  axis magnetization exhibits neither conventional field/temperature ( $H/T$ ) paramagnetic scaling nor Arrott-Noakes ferromagnetic critical scaling (20) (see fig. S7). Instead, the data scale in accordance with the Belitz-Kirkpatrick-Vojta (BKV) theory of metallic ferromagnetic quantum criticality (21). For temperatures  $< 9$  K and fields  $< 3$  T, the magnetization data scale as  $M/T^\beta$  versus  $H/T^{\beta+\gamma}$  (Fig. 2D), using BKV critical exponents ( $\beta = 1$ ,  $\gamma = 0.5$ ,  $\delta = 1.5$ ), behavior that has only otherwise been observed in  $\text{NiCoCr}_{0.8}$  (22). This scaling, extending over five orders of magnitude, indicates that  $\text{UTe}_2$  is a quantum critical ferromagnet, dominated by strong magnetic fluctuations. BKV theory applies to disordered metals and therefore, in principle, should not be applicable to  $\text{UTe}_2$ , which is in the clean limit (with a residual resistivity ratio of  $\sim 30$ ). Instead, a ferromagnetic quantum phase transition is expected to be first order in the clean limit (23). Therefore, the observation of quantum criticality in  $\text{UTe}_2$  calls for a different theory.

The transition from this correlated normal state to a superconducting ground state below the critical temperature  $T_c = 1.6$  K is robust and sharp, as is evident in the low-temperature  $\rho(T)$ , ac magnetization  $\chi(T)$  and specific heat  $C(T)$  data (Fig. 3). There is a large residual value of the Sommerfeld coefficient  $\gamma_0 = 55$  mJ/mol-K<sup>2</sup> in the superconducting state, or approximately half of the normal state value 110 mJ/mol-K<sup>2</sup>, from which it is immediately apparent that either a large fraction of the sample is not superconducting or half of the conduction electrons at the chemical potential in this material are not gapped by the superconducting transition; the latter is indicative of an unconventional pairing mechanism, such as what occurs in  $\text{UPt}_3$ ,  $\text{UCoGe}$ , and  $\text{UGe}_2$  (24, 25). There is little variation in the residual  $\gamma_0$  value between samples of  $\text{UTe}_2$  with slightly different  $T_c$  (fig. S12), suggesting that the large residual electronic density of states is likely an intrinsic, disorder-insensitive property of  $\text{UTe}_2$ . The normalized jump in  $C(T)$  at  $T_c$  is  $\Delta C/\gamma T_c = 2.5$ , which is much larger than the conventional Bardeen-Cooper-Schrieffer value of 1.43 expected from weak coupling, placing the system in the strong coupling regime; here,  $\gamma$  includes only the part that superconducts below  $T_c$  and is obtained by subtracting the residual value from the full value. For temperatures below  $T_c$ ,  $C(T)$  follows a power law, with the exponent  $n \sim 3.2$ , reflecting the presence of point nodes.

Perhaps the most pronounced sign of unconventional superconductivity is obvious in the upper critical field  $H_{c2}$  of this superconductor. The resistivity as a function of temperature for different magnetic fields applied along the three principal crystal axes is shown in Fig. 4. The  $H_{c2}$

<sup>1</sup>NIST Center for Neutron Research, National Institute of Standards and Technology, Gaithersburg, MD 20899, USA.

<sup>2</sup>Department of Physics, Center for Nanophysics and Advanced Materials, University of Maryland, College Park, MD 20742, USA. <sup>3</sup>Ames Laboratory, U.S. Department of Energy and Department of Physics and Astronomy, Iowa State University, Ames, IA 50011, USA. <sup>4</sup>Department of Materials Science and Engineering, University of Maryland, College Park, MD 20742, USA.

\*Corresponding author. Email: sran@umd.edu (S.R.); nbutch@umd.edu (N.P.B.)

is strongly anisotropic, with the value along  $b$  exceeding the two orthogonal directions by a factor of 4 at 1 K. The zero-temperature limit of  $H_{c2}$  along  $b$  well exceeds the highest measured magnetic field of 20 T, and we conservatively estimate a value of 40 T on the basis of the curvature of the critical field in UCoGe (26). The  $H_{c2}$  value is very sensitive to the alignment of magnetic field along the  $b$  axis (fig. S5).

The upper critical field of a conventional singlet superconductor is restricted by both of the orbital and paramagnetic pair-breaking effects. The zero-temperature orbital limit in superconductors is often well described by the Werthamer-Helfand-Hohenberg (WHH) theory  $H_{orb} = 0.7 dH_{c2}/dT_c|_{T_c} T_c$  (27). Although it can account for the response to field along the  $a$  axis, the WHH model otherwise disagrees drastically with our experimental results, most prominently along the  $b$  axis, where the slope of  $H_{c2}$  at  $T_c$  is  $\sim 17$  T/K along  $b$ , which leads to an expected  $H_{orb} = 20$  T for this direction. The conventional paramagnetic zero-temperature limit is given by  $H_{para} = 1.86 T_c$  (28), yielding  $H_{para} = 3$  T for  $UTe_2$ . In the zero-temperature limit, the experimental  $H_{c2}$  value well exceeds  $H_{para}$  in all three directions and by almost an order of magnitude along the  $b$  axis, excluding spin-singlet order parameters.

The violation of the orbital limit in directions perpendicular to the magnetic easy axis (the  $a$  axis) is consistent with the behavior of the ferromagnetic superconductors (29) and differs qualitatively from the relatively low  $H_{c2}$  values found in other paramagnetic triplet superconductors (8, 30). The unusual shape of the  $H_{c2}$  curve of  $UTe_2$  resembles those of UCoGe (26) and URhGe (31), in which ferromagnetic spin fluctuations are believed to mediate the superconducting pairs (25). Although the normal state of  $UTe_2$  is not magnetically ordered, the notable similarities suggest that its superconducting pairs are also mediated by ferromagnetic spin fluctuations, indicating that it is the end member of the series of ferromagnetic superconductors. When superconducting pairing is mediated by ferromagnetic spin fluctuations, the field dependence of the magnetization is coupled to the field dependence of the superconducting coupling strength (32), as verified in UCoGe and URhGe (33). The coupling strength  $\lambda$  as a function of magnetic field can be estimated based on the behavior of  $H_{c2}$  and  $\gamma$  (24). Especially prominent is the large increase in  $\lambda$  along the  $b$  axis of  $\sim 50\%$  (fig. S6), which far exceeds the field-induced enhancement of  $\lambda$  in UCoGe (33).

Further confirmation of spin-triplet pairing in  $UTe_2$  comes from NMR measurements, which are sensitive to internal magnetic fields (Fig. 3D). No change of the peak position is observed in the  $^{125}\text{Te}$ -NMR spectra between normal and superconducting states, leading to a temperature-independent value of the  $^{125}\text{Te}$  Knight shift  $K$ , which is proportional to the spin susceptibility of the quasiparticles forming the superconducting pairs. In singlet-paired superconductors,  $K$  decreases below  $T_c$ , whereas in  $UTe_2$ ,  $K$  remains

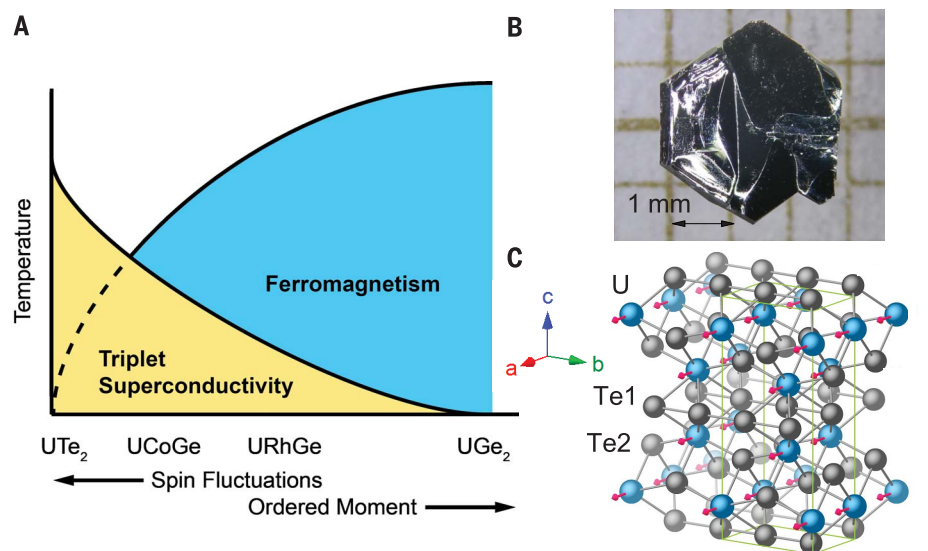


**Fig. 1. Structure of  $UTe_2$ .** (A) Global phase diagram of ferromagnetic superconductors;  $UTe_2$  is located at the paramagnetic end of the series. (B) A photo of a single crystal of  $UTe_2$  grown using chemical vapor transport method on the millimeter scale. (C) Crystal structure of  $UTe_2$ , with U atoms in blue and Te atoms in gray. The U atoms sit on chains parallel to the [100]  $a$  axis, which coincides with the magnetic easy axis, illustrated by the magenta arrows.

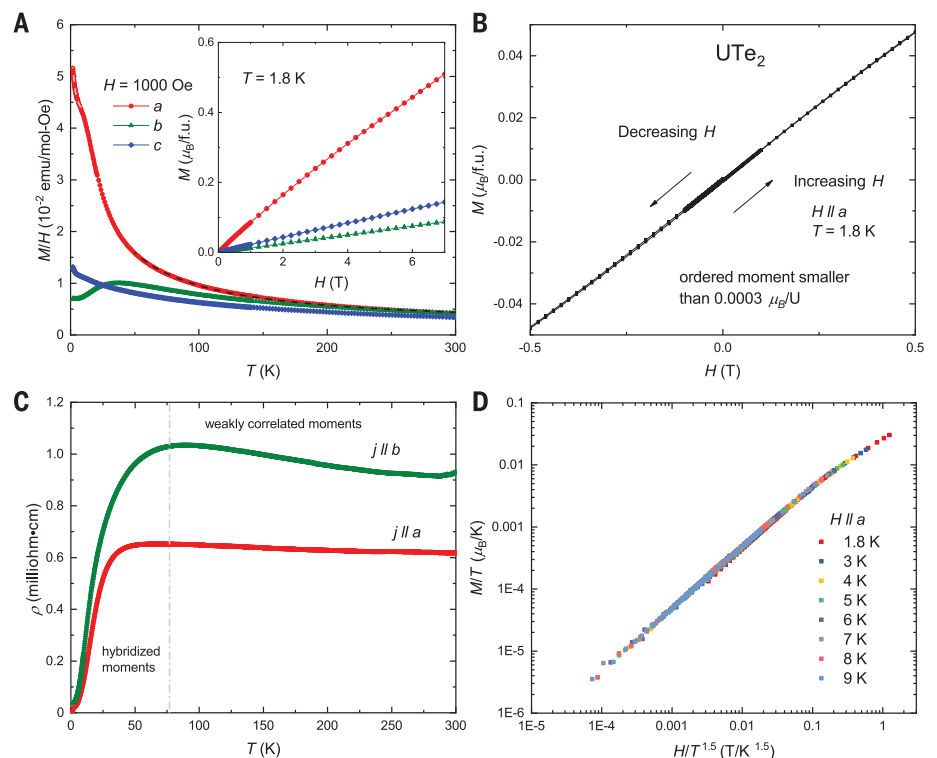


**Fig. 2. Normal state properties of  $UTe_2$ .** (A) Temperature dependence of magnetization for three different directions of magnetic field of 0.1 T. For the field in  $a$  direction, the gray dashed line is the fit to the power law in the low-temperature region, whereas the black dashed line is the fit to the Curie-Weiss law in the high-temperature region. (Inset) Magnetization as a function of applied field in three directions at 1.8 K. (B) Magnetization data at 1.8 K upon increasing and decreasing magnetic field in the low field range showing no hysteresis. The upper bound for an ordered moment is  $0.0003 \mu_B/U$  obtained from the zero field magnetization value. (C) Temperature dependence of electric resistivity data in zero magnetic field with electric current applied along  $a$  and  $b$  axes. (D)  $M/T$  as a function of  $H/T^{1.5}$  for different temperatures. All the data collapse onto a single line. This scaling corresponds to the BKV theory of metallic ferromagnetic quantum criticality (see text).

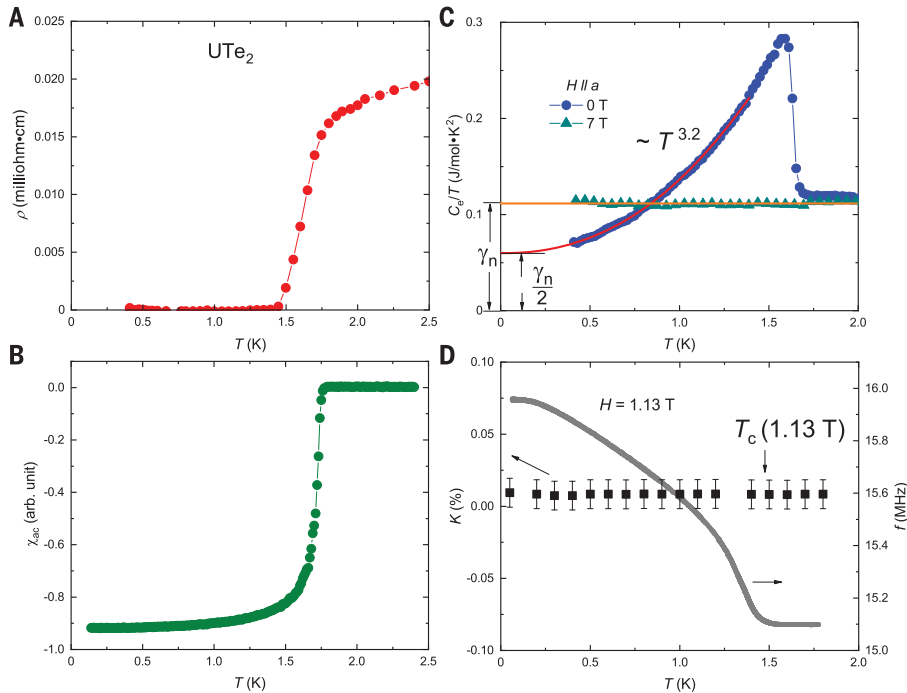


**Fig. 3. Superconducting state properties of UTe<sub>2</sub>.** Temperature dependence of (A) resistivity and (B) ac magnetization data at low temperatures showing bulk superconductivity. (C) Electric contribution to heat capacity (phonon contribution has been subtracted as explained in the supplementary materials) in zero field and 7 T, divided by temperature, is shown as a function of temperature, illustrating  $\gamma$  in the superconducting and normal states. Magnetic field is applied along the *a* axis. (D) Temperature dependence of <sup>125</sup>Te NMR Knight shift *K* below and near *T<sub>c</sub>* of powdered UTe<sub>2</sub> sample (left axis) and of the resonance frequency *f* of the NMR tank circuit confirming the superconducting state and *T<sub>c</sub>* (right axis). *H* = 1.13 T.

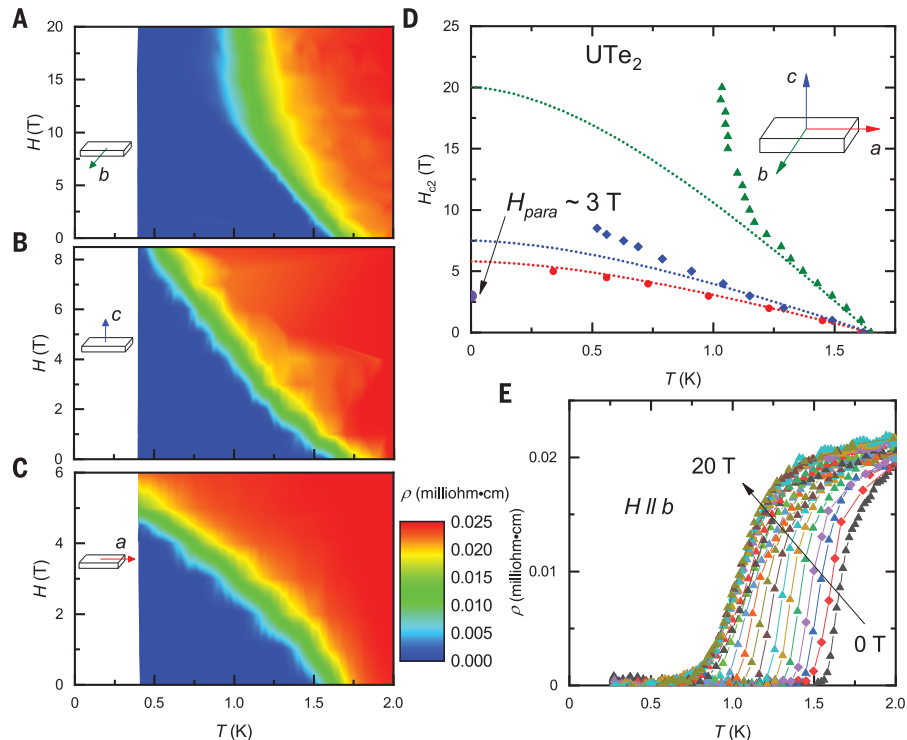


**Fig. 4. Upper critical field *H<sub>c2</sub>* of UTe<sub>2</sub>.** (A to C) Color contour plots of resistivity value as a function of temperature and magnetic field, with magnetic fields applied along (A) the *b* axis, (B) the *c* axis, and (C) the *a* axis. The current is applied along the *a* axis. (D) The *H<sub>c2</sub>* value as a function of *T* in three directions. Dotted lines represent the WHH fit of the *H<sub>c2</sub>* data. (E) Temperature-dependent resistivity data in magnetic fields applied along the *b* axis up to 20 T. Curves were measured using a constant magnetic field interval of 1 T.

constant on passing through *T<sub>c</sub>*, signifying that the superconducting pair is a spin triplet (34, 35). The unconventional nature of the superconductivity in UTe<sub>2</sub> is also observed in the temperature dependence of <sup>125</sup>Te nuclear spin-lattice relaxation rate  $1/T_1$  (fig. S16).  $1/T_1$  shows a steep drop below  $\sim 1$  K without showing a Hebel-Slichter coherence peak in  $1/T_1$  just below *T<sub>c</sub>*, which is expected for conventional BSC superconductors. The temperature dependence of  $1/T_1$  below *T<sub>c</sub>* follows a power law behavior  $1/T_1 \sim T^6$  which is close to the  $1/T_1 \sim T^5$  relation expected from the point-node gap structure (36, 37), consistent with the results of the specific heat measurement.

Having established clear evidence for spin-triplet pairing, one possible superconducting pairing symmetry consistent with a large fraction of ungapped electronic states of UTe<sub>2</sub> is the nonunitary triplet state, in which a two-component superconducting order parameter has two different energy gaps. However, such a state is generally not expected for paramagnetic, orthorhombic systems with strong spin-orbit coupling—this scenario applies to UTe<sub>2</sub> unless the effective spin-orbit coupling is demonstrated to be weak owing to special circumstances. No other standard archetype fits all measured properties of UTe<sub>2</sub>, and any candidate state must account for the large field anisotropy, nodal gap structure, and the large residual electronic density of states, which are by themselves unusual. The high upper critical field itself suggests that the superconducting state resembles a condensate of equal spin pairs. One general possibility is band-selective superconductivity in a highly anisotropic electronic structure having multiple Fermi surfaces. Ongoing electronic structure measurements will help to determine whether such a description is applicable here. Regardless, explaining the relevance of ferromagnetic quantum criticality and the role of spin fluctuations will require further theoretical work.

The discovery of this superconducting state opens the door to advances in the study of spin-triplet pairing, topological electronic states, and their application to quantum information technology. As a paramagnetic version of ferromagnetic superconductors, UTe<sub>2</sub> is a promising topological superconductor (38) and may host Majorana excitations that can be detected by angle-resolved photoemission spectroscopy or scanning tunneling microscope (39).

#### REFERENCES AND NOTES

1. M. Sato, Y. Ando, *Rep. Prog. Phys.* **80**, 076501 (2017).
2. C. Beenakker, *Annu. Rev. Condens. Matter Phys.* **4**, 113–136 (2013).
3. S. D. Sarma, M. Freedman, C. Nayak, *npj Quantum Inf.* **1**, 15001 (2015).
4. J. Alicea, *Rep. Prog. Phys.* **75**, 076501 (2012).
5. A. Y. Kitaev, *Phys. Uspekhi* **44** (10S), 131–136 (2001).
6. N. Read, D. Green, *Phys. Rev. B* **61**, 10267–10297 (2000).
7. R. M. Lutchyn *et al.*, *Nat. Rev. Mater.* **3**, 52–68 (2018).
8. A. P. Mackenzie, Y. Maeno, *Rev. Mod. Phys.* **75**, 657–712 (2003).
9. C. Kallin, A. J. Berlinsky, *J. Phys. Condens. Matter* **21**, 164210 (2009).
10. Y. Maeno, S. Kittaka, T. Nomura, S. Yonezawa, K. Ishida, *J. Phys. Soc. Jpn.* **81**, 011009 (2012).
11. J. D. Strand *et al.*, *Science* **328**, 1368–1369 (2010).
12. E. R. Schermm, W. J. Gannon, C. M. Wishne, W. P. Halperin, A. Kapitulnik, *Science* **345**, 190–193 (2014).
13. S. S. Saxena *et al.*, *Nature* **406**, 587–592 (2000).

14. D. Aoki *et al.*, *Nature* **413**, 613–616 (2001).
15. N. T. Huy *et al.*, *Phys. Rev. Lett.* **99**, 067006 (2007).
16. D. Aoki, K. Ishida, J. Flouquet, *J. Phys. Soc. Jpn.* **88**, 022001 (2019).
17. S. Ikeda *et al.*, *J. Phys. Soc. Jpn.* **75** (suppl), 116–118 (2006).
18. H. Noël, M. Potel, R. Troc, L. Shlyk, *J. Solid State Chem.* **126**, 22–26 (1996).
19. G. R. Stewart, *Rev. Mod. Phys.* **56**, 755–787 (1984).
20. N. P. Butch, M. B. Maple, *Phys. Rev. Lett.* **103**, 076404 (2009).
21. T. R. Kirkpatrick, D. Belitz, *Phys. Rev. B* **91**, 214407 (2015).
22. B. C. Sales *et al.*, *npj Quantum Materials* **2**, 33 (2017).
23. M. Brando, D. Belitz, F. M. Grosche, T. R. Kirkpatrick, *Rev. Mod. Phys.* **88**, 025006 (2016).
24. R. Joynt, L. Taillefer, *Rev. Mod. Phys.* **74**, 235–294 (2002).
25. V. P. Mineev, *Phys. Uspekhi* **60**, 121–148 (2017).
26. D. Aoki *et al.*, *J. Phys. Soc. Jpn.* **78**, 113709 (2009).
27. E. Helfand, N. R. Werthamer, *Phys. Rev.* **147**, 288–294 (1966).
28. A. M. Clogston, *Phys. Rev. Lett.* **9**, 266–267 (1962).
29. V. P. Mineev, *Phys. Rev. B* **95**, 104501 (2017).
30. Z. F. Weng *et al.*, *Phys. Rev. Lett.* **117**, 027001 (2016).
31. F. Lévy, I. Sheikin, B. Grenier, A. D. Huxley, *Science* **309**, 1343–1346 (2005).
32. V. P. Mineev, *Phys. Rev. B* **83**, 064515 (2011).
33. B. Wu *et al.*, *Nat. Commun.* **8**, 14480 (2017).
34. H. Tou *et al.*, *Phys. Rev. Lett.* **77**, 1374–1377 (1996).
35. K. Ishida *et al.*, *Nature* **396**, 658–660 (1998).
36. J. Yang, Z. T. Tang, G. H. Cao, G. Q. Zheng, *Phys. Rev. Lett.* **115**, 147002 (2015).
37. K. Katayama *et al.*, *J. Phys. Soc. Jpn.* **76**, 023701 (2007).
38. A. K. C. Cheung, S. Raghu, *Phys. Rev. B* **93**, 134516 (2016).
39. J. D. Sau, S. Tewari, *Phys. Rev. B* **86**, 104509 (2012).
40. S. Ran, Replication data for: Nearly ferromagnetic spin-triplet superconductivity, Version 1, Harvard Dataverse (2019); <https://doi.org/10.7910/DVN/UJAFUC>.

#### ACKNOWLEDGMENTS

We thank W. Fuhrman, Y.-T. Hsu, T. Kong, S. Raghu, J. Sau, Y. Wang, S.-L. Xu, and V. Yakovenko for helpful discussions. We also thank H. Hodovanets for assistance during our experiments. **Funding:** Research at the University of Maryland was supported by the National Science Foundation Division of Materials Research Award DMR-1610349, U.S. Department of Energy (DOE) Award DE-SC-0019154, Air Force Office of Scientific Research Award FA9550-14-1-0332, and the Gordon and Betty Moore Foundations EPIQS Initiative through Grant GBMF4419. Research at Ames Laboratory was supported by the U.S. Department of

Energy (DOE), Office of Basic Energy Sciences, Division of Materials Sciences and Engineering. Ames Laboratory is operated for the U.S. DOE by Iowa State University under Contract DE-AC02-07CH11358. **Author contributions:** S.R. and N.P.B. conceived of and designed the study. S.R. and S.R.S. synthesized the single crystalline samples. S.R., C.E., I.-L.L., H.K., and J.P. performed the electrical resistivity measurements. S.R., C.E., and T.M. performed the specific heat measurements. S.R., S.R.S., and M.Z. performed the magnetization measurements. S.R. and N.P.B. performed the neutron scattering measurements. Q.-P.D. and Y.F. performed the NMR measurements. All authors contributed to the preparation of the manuscript. **Competing interests:** The authors declare no competing interests. **Data and materials availability:** Data are available at Harvard Dataverse (40).

#### SUPPLEMENTARY MATERIALS

[science.sciencemag.org/content/365/6454/684/suppl/DC1](http://science.sciencemag.org/content/365/6454/684/suppl/DC1)  
Materials and Methods  
Supplementary Text  
Figs. S1 to S16

29 October 2018; accepted 12 July 2019  
10.1126/science.aav8645

## Nearly ferromagnetic spin-triplet superconductivity

Sheng Ran, Chris Eckberg, Qing-Ping Ding, Yuji Furukawa, Tristin Metz, Shanta R. Saha, I-Lin Liu, Mark Zic, Hyunsoo Kim, Johnpierre Paglione and Nicholas P. Butch

*Science* **365** (6454), 684-687.  
DOI: 10.1126/science.aav8645

### An unusual superconductor

In conventional, and in many unconventional, superconductors, the electrons that form Cooper pairs have spins pointing in opposite directions. An applied magnetic field can easily "break" such pairs—and destroy superconductivity—by aligning both spins in the same direction. In contrast, spin-triplet superconductors are much more resilient to magnetic fields. Very few candidates for such materials have been discovered. Ran *et al.* add to this select group by observing signatures of spin-triplet superconductivity, including a very large and anisotropic upper critical magnetic field, in the material UTe<sub>2</sub>. Because spin-triplet superconductors may naturally exhibit topological superconductivity, this material may also be of interest in quantum computing.

*Science*, this issue p. 684

#### ARTICLE TOOLS

<http://science.sciencemag.org/content/365/6454/684>

#### SUPPLEMENTARY MATERIALS

<http://science.sciencemag.org/content/suppl/2019/08/14/365.6454.684.DC1>

#### REFERENCES

This article cites 39 articles, 3 of which you can access for free  
<http://science.sciencemag.org/content/365/6454/684#BIBL>

#### PERMISSIONS

<http://www.sciencemag.org/help/reprints-and-permissions>

Use of this article is subject to the [Terms of Service](#)